

Incorporation of Preprocedural PET into CT-Guided Radiofrequency Ablation of Hepatic Metastases: a Nonrigid Image Registration Validation Study

Peng Lei,^{1,2} Omkar Dandekar,^{1,3} David Widlus,¹ and Raj Shekhar^{1,2,3}

This study evaluates the accuracy of augmenting initial intraprocedural computed tomography (CT) during radiofrequency ablation (RFA) of hepatic metastases with preprocedural positron emission tomography (PET) through a hardware-accelerated implementation of an automatic nonrigid PET–CT registration algorithm. The feasibility of augmenting intraprocedural CT with preprocedural PET to improve localization of CT-invisible but PET-positive tumors with images from actual RFA was explored. Preprocedural PET and intraprocedural CT images from 18 cases of hepatic RFA were included. All PET images in the study originated from a hybrid PET/CT scanner, and PET–CT registration was performed in two ways: (1) direct registration of preprocedural PET with intraprocedural CT and (2) indirect registration of preprocedural CT (i.e., the CT of hybrid PET/CT scan) with intraprocedural CT. A hardware-accelerated registration took approximately 2 min. Calculated registration errors were 7.0 and 8.4 mm for the direct and indirect methods, respectively. Overall, the direct registration was found to be statistically not distinct from that performed by a group of clinical experts. The accuracy, execution speed, and compactness of our implementation of nonrigid image registration suggest that existing PET can be overlaid on intraprocedural CT, promising a novel, technically feasible, and clinically viable approach for PET augmentation of CT guidance of RFA.

KEY WORDS: CT, Radiofrequency ablation, Image registration, Mutual information, PET

BACKGROUND

The liver is a common site of metastatic tumors. Most (80%–85%) hepatic malignancies are not suitable for surgical resection because of size, number, anatomic distribution, inadequate volume of viable liver tissue, or extrahepatic involvement.^{1,2} Percutaneous radiofrequency ablation (RFA) has emerged recently as a treatment of choice for metastatic tumors unsuitable for surgical

resection.³ A minimally invasive procedure guided by intraprocedural imaging devices, RFA is performed by placing a needle-like RF applicator into the tumor to deliver high-frequency alternating electrical current that thermally destroys cancerous cells.⁴ Favorable patient outcomes have been reported for RFA of hepatic metastases, with 1-, 2-, and 3-year survival rates of 93%, 69%, and 46%, respectively.⁵

Successful RFA depends on complete malignancy ablation that requires optimal placement of the RF applicator inside the tumor.⁶ The potential inability of currently available 2-dimensional (2D) imaging modalities (ultrasound and fluoroscopy) to clearly visualize and precisely localize the targeted malignancy in the 3D space complicates the placement of the RF applicator. With the advent of multidetector computed tomography (CT), volumetric CT with multiplanar reformations is increasingly used for intraprocedural guidance and has been reported to

¹From the Department of Diagnostic Radiology and Nuclear Medicine, School of Medicine, University of Maryland, 22 S. Greene St., Baltimore, MD, 21201, USA.

²From the Fischell Department of Bioengineering, University of Maryland, College Park, MD, 20742, USA.

³From the Department of Electrical and Computer Engineering, University of Maryland, College Park, MD, 20742, USA.

Correspondence to: Raj Shekhar, Department of Diagnostic Radiology and Nuclear Medicine, School of Medicine, University of Maryland, 22 S. Greene St., Baltimore, MD, 21201, USA; fax: +1-410-7068724; e-mail: rshkhar@umm.edu

Copyright © 2009 by Society for Imaging Informatics in Medicine

doi: 10.1007/s10278-009-9204-x

greatly improve applicator placement in hepatic RFA because it provides a detailed 3D anatomic roadmap.⁷ The low sensitivity of intraprocedural CT (most often without contrast because of time and clinical constraints), however, remains a limitation, rendering most lesions inconspicuous during the ablative procedure. Even contrast-enhanced CT (CECT) has been shown to miss hepatic lesions with abnormal metabolic activity.⁸ The inherent uncertainty in localizing an inconspicuous malignancy may lead to incomplete and misdirected treatment and may contribute to the local recurrence documented in up to 39% of RFA-treated hepatic malignancies.^{6,9}

Positron emission tomography (PET) using 2-[¹⁸F]-fluoro-2-deoxyglucose (¹⁸F-FDG) as radiotracer is more sensitive and specific than CT in detecting hepatic metastases and even RFA-treated residual tumors, both colorectal and noncolorectal.^{2,10,11} In a meta-analysis of hepatic metastasis detection studies, Kinkel et al. compared the sensitivities of ultrasound, CECT, magnetic resonance imaging, and PET and found that in studies with >85% specificity, the sensitivities were 55%, 72%, 76%, and 90%, respectively.¹² Noncontrast CT (NCCT), the protocol commonly used in RFA, has even lower sensitivity than CECT (55% versus 72%), as reported in a multi-institutional study.¹³ Although frequently used in preprocedural planning and postprocedural follow-up, PET images are rarely used for image guidance. The low-resolution low-acquisition speed and radiation exposure of PET restrict its deployment in interventional procedure suites. Therefore, the interventional radiologist must mentally project preprocedural PET findings onto intraprocedural CT roadmap to localize the malignancy—a subjective task that is dependent on operator expertise and susceptible to error. If the preprocedural PET image could be overlaid on the latest structural CT image automatically in procedure suites, the complementary functional information in PET will augment the anatomic roadmap of CT, and the fused PET–CT images could greatly improve the target localization.¹⁴

Fusion of PET and corresponding CT images is now available through hybrid PET/CT scanning, which achieves alignment/fusion mechanically by sequentially performing the two scans in a single session to minimize temporal and spatial differences.¹⁵ However, PET scanning, by either conventional stand-alone PET or hybrid PET/CT, cannot

be repeated intraprocedurally because of time and logistic challenges, as well as radiation exposure risks.¹⁶ Another simple approach to image registration is to use fiducials visible in both PET and CT images. Wahl et al. reported an “anatometabolic” tumor imaging method using both external artificial markers (filled with ¹⁸F-FDG) attached to the patient’s skin and internal anatomic landmarks identified in PET and CT.¹⁷ Adoption of this method from radiotherapy into RFA has limitations. Manual identification of anatomic landmarks is too time consuming to be used routinely during RFA. Moreover, nonrigid registration has been shown to be necessary for successful soft tissue deformation modeling¹⁸, especially the complex abdominal deformation in hepatic RFA. Nonrigid registration requires a large number of landmarks to accurately recover misalignment—a condition difficult to satisfy for the liver.

In the last decade, automatic multimodality nonrigid image registration techniques have emerged that do not involve landmarks. These techniques compute a cost function, such as mutual information (MI), derived from image intensities and determine the transformation for which the cost function is at a maximum (or minimum, if that is the goal), coinciding with perfect spatial alignment between the images.^{19,20} Numerous recent studies have focused on MI-based PET–CT registration of various anatomies.^{21–25}

Existing nonrigid image registration algorithms²⁶ have been validated for the registration of whole-body (thorax and abdomen) PET and CT images²³ and CECT with ultralow-dose NCCT.²⁷ Registering images of the liver specific to RFA and employing it intraprocedurally present newer challenges: large, complex, and nonrigid motion and deformation in the abdomen; absence of bony structures to provide an “anchor” for registration; fewer image slices as a result of relatively small longitudinal coverage; poorer image quality of intraprocedural CT because of the absence of contrast enhancement; etc.

This study focuses on the accuracy of MI-based nonrigid registration of PET and NCCT images of the liver obtained in association with RFA procedures. The results show that fast and accurate PET–CT registration during RFA is possible and that this capability can be integrated into the current CT-guided RFA workflow (Fig. 1) for improved targeting of hepatic lesions and their ablation with much greater certainty.

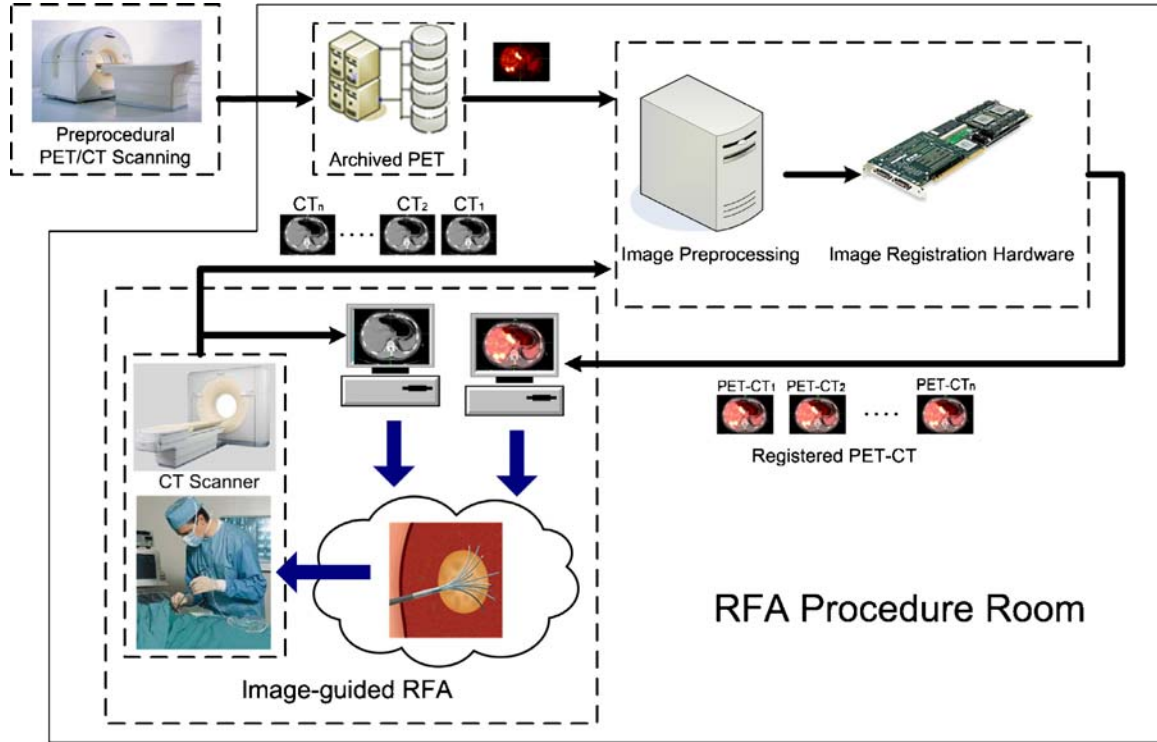


Fig 1. Proposed workflow for incorporating preprocedural PET into intraprocedural CT guidance of hepatic RFA.

METHODS

Registration Algorithm

The registration algorithm and its hardware-accelerated implementation used in this study have been validated for the registration of whole-body (thorax and abdomen) PET and CECT images.^{23,26,28} It is based on maximization of normalized MI (NMI) similarity measure²⁹, a variant of MI, which is less sensitive to the degree of image overlap and uses a hierarchical coarse-to-fine nonrigid model to simulate the deformation. For the reference image (RI) and the floating image (FI), where $p_R(a)$ and $p_F(b)$ are the probability density function, the entropy is defined as

$$H(R) = -\sum_a p_R(a) \log p_R(a)$$

$$H(F) = -\sum_b p_F(b) \log p_F(b)$$

The entropy of the joint distribution is defined as

$$H(R, F) = -\sum_{a,b} p_{R,F}(a, b) \log p_{R,F}(a, b)$$

The NMI is defined as

$$\text{NMI}(R, F) = \frac{H(R) + H(F)}{H(R, F)}$$

The registration iteratively searches for the optimal geometrical warping of RI so that the NMI between RI and FI is maximized, which coincides with the alignment of the two images.

First, a six-parameter (three translational and three rotational components) rigid-body registration between RI and FI is performed to recover the global misalignment. The calculated transformation is denoted as T^0 . Next, the multilevel nonrigid registration uses an octree-based scheme to progressively subdivide the RI into subvolumes. At each level i , a subvolume from previous level $i-1$ is further divided into eight subvolumes (a total of 8^{i-1} subvolumes for level i). The concept of image subdivision is illustrated in Figure 2. The maxi-

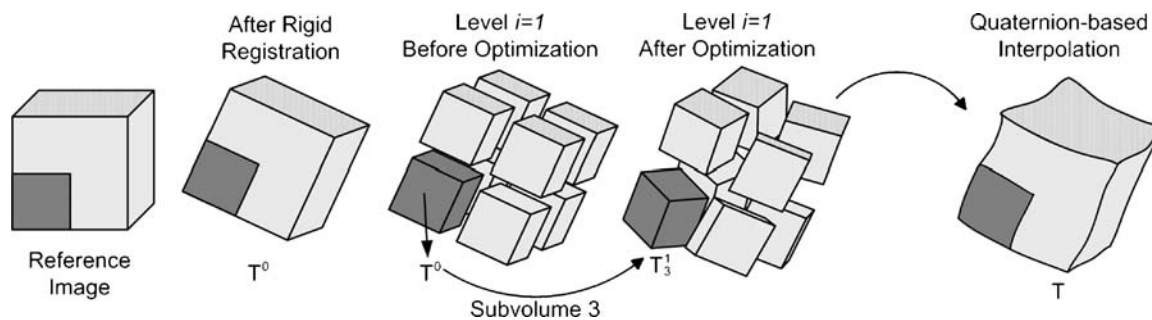


Fig 2. Illustration of the image subdivision scheme of the registration.

num number of levels is limited by a predefined minimal voxel number (16^3) in the subvolume to keep the computation of NMI statistically significant. Each subvolume j is individually registered with the FI (the calculated transformation is denoted as T_j^i), starting from the calculated transformation of its parent subvolume at previous level $i-1$, which contains the subvolume j . The registration of subvolume also uses six parameters and is NMI-based. This registration process is continued until the process converges (change of $NMI < 0.1\%$) or the predefined maximum number (200) of iterations is reached. Thus, this registration process hierarchically matches all local subvolumes of the RI with the entire FI. The final cumulative nonrigid transformation T is computed by interpolation of the individual subvolume transformations at the final subdivision level. In the interpolation scheme, quaternions are used to represent the 3D rotational pose as a single rotation angle about an axis in the 3D space.³⁰ The quaternion representation permits direct interpolation of rotations.

In this study, intraprocedural NCCT and preprocedural PET were considered as RI and FI, respectively. Both PET and NCCT images were cropped to remove most background voxels, and their intensities were converted to an 8-bit scale. NCCT images were smoothed with an anisotropic diffusion filter to reduce noise.^{31,32} All preprocessing procedures (smoothing, cropping, and bit number reduction) were applied only to intermediate images used during registration, and the registered images were output by applying the transformation T to the original PET images. An initial seed alignment of the two images along the longitudinal axis (i.e., head-to-toe direction) was manually provided to compensate for different

scanner coordinates and to ensure reasonable overlap of common regions in both images.

Registration Strategy

In this study, PET-CT registration was accomplished in two ways (Fig. 3). The first (direct) method uses direct registration of preprocedural PET with intraprocedural NCCT to determine the deformation between the two images. With the direct method, preprocedural PET (from either stand-alone PET or hybrid PET/CT) can be registered to each intraprocedural NCCT volume and overlaid on the NCCT to augment the anatomic map with functional information. Because of the rapid adoption of hybrid PET/CT scanners, preprocedural PET scans often have

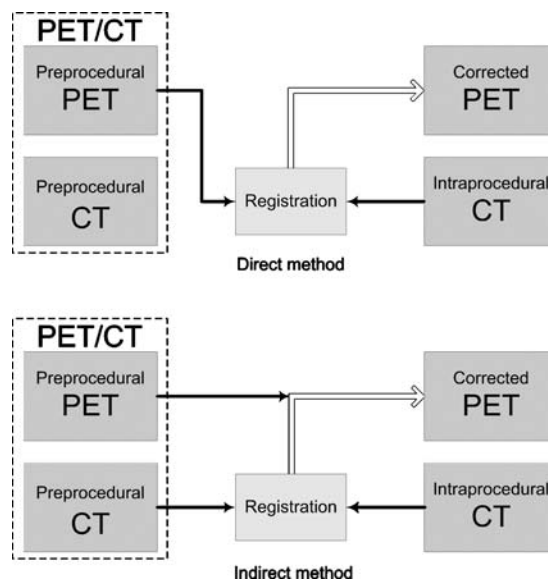


Fig 3. Schematic illustration of direct and indirect methods of registering preprocedural PET and intraprocedural CT.

corresponding mechanically aligned CT scans. The second (indirect) method, applicable only to hybrid PET/CT scans, such those as in our study, replaces preprocedural PET with preprocedural CECT in the direct method and registers preprocedural CECT with intraprocedural NCCT to determine the deformation and then corrects preprocedural PET according to the result of CT–CT registration. The indirect method assumes perfect native alignment of preprocedural PET and preprocedural CECT from the PET/CT scanner and benefits from avoiding the use of low-resolution and low signal-to-noise ratio (SNR) PET images in the PET–CT registration. However, the assumption of perfect native alignment may not always hold true, as shown by many studies. Despite using optimal respiration protocols, breathing-induced misregistration of up to 12 mm has been reported in hybrid PET/CT scans.³³ A head-to-head comparison for the specific instance of hepatic RFA was included in this study to determine whether direct registration or indirect registration is the more appropriate strategy.

Implementation

The registration was performed on a Dell Precision 670 Workstation (Dell, Inc., Round Rock, TX, USA; Intel dual Xeon processor at 3.59 GHz, 2.0 G DDRAM, FSB at 800 MHz, Microsoft Windows XP Professional Edition operation system) PC. The computation of NMI, which can take up to 99.9% of execution time³⁴, was performed by a previously reported²⁸ field programmable gate array (FPGA)–based implementation on an add-on FPGA board (DN7000K10PCI; The Dini Group, La Jolla, CA, USA), equipped with 1-GB double-data-rate DRAM and running at 200-MHz clock speed. To meet the performance and accuracy requirements of the current application, as well as to make effective use of the chosen computing platform, this implementation was tuned, through software- and hardware-level code optimization, as previously described.³⁵ During the registration, the downhill simplex optimization routine (hosted on the PC) generated candidate transformations. The optimized FPGA implementation applied this transformation to images and computed the NMI corresponding to that transformation. The optimization terminated when NMI was maximized.

Validation

Because no reference solution exists for the proposed image registration, the opinions of three interventional radiologists experienced in evaluating PET and CT images were regarded as the performance benchmark. The three experts identified four landmarks (dome of liver, inferior tip of liver, and upper and lower poles of right kidney) in each of the PET and NCCT images of the 18 image pairs. The algorithm provides a one-to-one correspondence between any point in the NCCT image space, including the four landmarks, to a point in the PET image space. Because experts differ slightly, our validation tested whether replacing any single expert with the algorithm made any statistical difference in interexpert variability. If the interexpert variability increased, the algorithmic registration’s capability in eliminating misalignment would be considered inferior to that of registration achieved by manual identification of corresponding points in PET and NCCT images by a human expert.

Figure 4 is a schematic illustration of our validation approach. Experts used custom display software with 3D navigation, zoom, and window/level functionalities to mark these points. For each landmark, a test point (CT_{TEST}) was determined as the average of expert identifications (centroid) of the same landmark in intraprocedural NCCT. CT_{TEST} maps to PET_{E1} , PET_{E2} , and PET_{E3} in the preprocedural PET according to the identification of the three experts (T_{E1} , T_{E2} , and T_{E3}) and PET_{ALGO} , according to the transformation field derived from the nonrigid registration (T_{ALGO}). PET_{EXPERT} represents the mean location (centroid) of PET_{E1} , PET_{E2} , and PET_{E3} . The mean error between PET_{EXPERT} and PET_{ALGO} , averaged over all landmarks and cases, was computed to determine the target registration error (TRE). To further evaluate the algorithm’s performance in the context of interexpert variability, the four locations in PET (three experts and one algorithm) were assigned to four separate groups of three locations each: reference group (PET_{E1} , PET_{E2} , and PET_{E3}), test group 1 (PET_{ALGO} , PET_{E2} , and PET_{E3}), test group 2 (PET_{E1} , PET_{ALGO} , and PET_{E3}), and test group 3 (PET_{E1} , PET_{E2} , and PET_{ALGO}). The variability of locations was calculated for each group. If the group variability of test groups 1, 2, and 3 was statistically similar to that of the

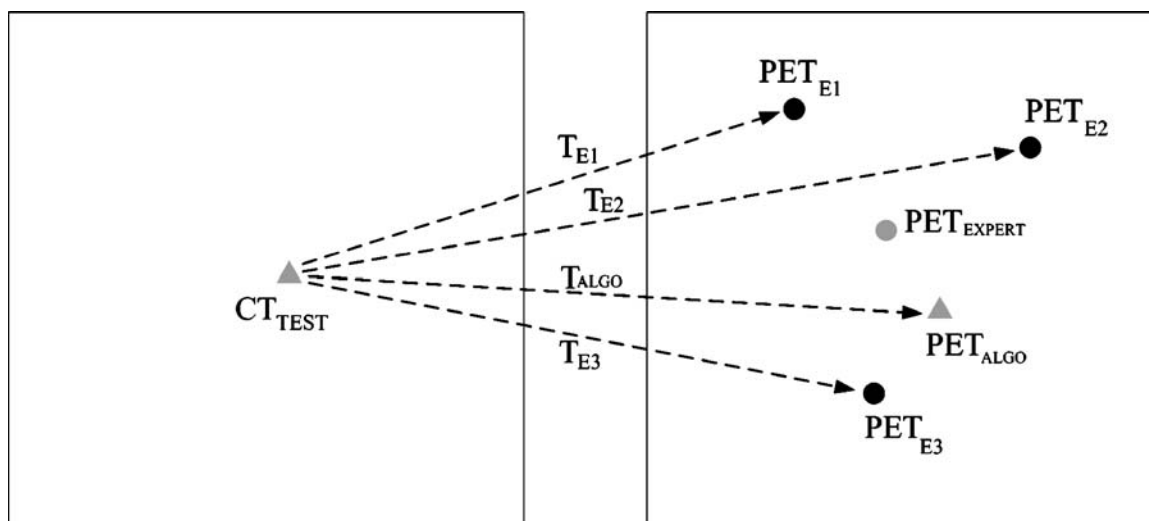


Fig 4. Test landmark and the validation approach. CT_{TEST} test landmark in CT; T_{E1} , T_{E2} , T_{E3} transformations of the test landmark determined by experts 1, 2, and 3, respectively; PET_{E1} , PET_{E2} , PET_{E3} locations of the test landmark identified in PET image space independently by experts 1, 2, and 3, respectively; T_{ALGO} the test landmark transformation determined by algorithm; PET_{ALGO} the landmark location predicted by algorithm; PET_{EXPERT} calculated as average of PET_{E1} , PET_{E2} , and PET_{E3} .

reference group, we concluded that the algorithm and experts agreed on the PET location of a specific landmark in NCCT. Each expert's landmark identification was considered independent. A one-sided sign test, appropriate for studies with small sample size, was conducted to evaluate if the median distance among locations in a group was less than or equal to the median distance among locations in the reference group. For all the tests, $P < 0.01$ was the criterion to reject the null hypothesis and indicated a statistically significant difference.

Data Acquisition

This retrospective study, with a protocol approved by our institutional review board, used archived images of patients who had undergone hepatic RFA under CT guidance at our medical center. The patient population included six women and seven men (median age, 60 years; range, 45–85 years) who had hepatic metastases (eight from colorectal cancer; five from other primary cancers). These patients were selected for this study by staff interventional radiologists experienced in RFA but not familiar with the workings of the registration algorithm. Inclusion criteria were the availability of preprocedural PET/CT (from a hybrid scanner) and intraprocedural NCCT scans

with no operative resection between PET and NCCT imaging. Each intraprocedural NCCT and the most recent preprocedural PET formed input datasets for registration. The average interval between the PET/CT scanning and the procedure was 31 ± 13 days. For patients with multiple RFA procedures, images associated with only those procedures separated by more than 2 months were included to ensure significant anatomic difference between the two cases. Overall, 18 pairs of preprocedural PET and intraprocedural CT sets were identified and included in this study. Of these, 13 represented the initial procedure in 13 patients. The remaining five originated from repeat procedures. No PET or CT dataset was duplicated when forming image pairs.

Preprocedural PET and CT scans were obtained with a hybrid PET/CT scanner (Brilliance 16, Philips Medical Systems, Cleveland, OH, USA). ^{18}F -FDG, with a dose range of 11–16 mCi, was administered intravenously 60 min before PET scanning, which lasted 25–35 min (five to seven bed positions, 5 min per bed position, scanning from the base of the skull to the midhigh) and was performed with the patient breathing normally. Preprocedural PET scans had a size of 150×150 samples axially and 187–240 slices longitudinally, with a voxel size of $4.0 \times 4.0 \times 4.0$ mm. The preprocedural CECT scans were acquired in the

helical mode at 120 kV tube voltage and 400 mA tube current settings. Patients were instructed to breathe gently during CT acquisition. The preprocedural CECT scans had a size of 512×512 samples axially and 192–233 slices longitudinally, with a voxel size of $1.18 \times 1.18 \times 4.0$ – 5.0 mm.

Intraprocedural abdominal NCCT scans for guiding the RF applicator were obtained at the beginning of the procedure under gentle respiration. Three stand-alone CT scanners (Brilliance 64 and Brilliance 40, Philips Medical Systems, Cleveland, OH, USA; and Toshiba Xpress/SX, Toshiba America Medical Systems, Tustin, CA, USA) were utilized in helical mode, at 80–120 kV tube voltage and 100–350 mA (median 175 mA) tube current settings. The intraprocedural NCCT scans had a size of 512×512 samples axially and 35–82 slices longitudinally, with a voxel size of 0.78 – 1.17×0.78 – 1.17×4 – 5 mm.

RESULTS

The algorithm converged successfully in all 18 cases and results of registration were evaluated both qualitatively and quantitatively. Qualitative evaluation included visual assessment of improvement in image alignment by clinical experts. No visually detectable gross misregistration, whether near the liver boundary or in the liver parenchyma, was found in any case. An example of registration using the direct method is presented in Figure 5. Axial, coronal, and sagittal views through the preprocedural PET and intraprocedural CT, as well as fused PET–CT images before and after nonrigid registration, are shown. In all three views, nonrigid registration provided image alignment superior to that of unregistered fusion images. Nonrigid registration corrected the misalignment of anatomic landmarks and lesions.

The TRE derived from the mean of $|\text{PET}_{\text{ALGO}} - \text{PET}_{\text{EXPERT}}|$ over all patients and landmarks was 7.0 (direct method) and 8.4 mm (indirect method). This result is comparable with the accuracy reported earlier for nonrigid 3D PET–CT registration of whole-body images²³, indicating that the registration algorithm's accuracy was independent of the anatomy.

Table 1 presents interexpert variability (i.e., group variability) in the identification of each of the four landmarks averaged over 18 image pairs

by the direct method. The table also presents the overall interexpert variability (last row) without differentiating among landmarks. The sign test showed no statistically significant difference between the reference group and any of the test groups (i.e., all test group values lay within the interquartile range of the reference group), indicating that the algorithm's solutions were not significantly statistically different from those of the experts. A similar analysis by landmarks showed no statistically significant difference between the algorithm and the three experts for three of the four landmarks. For the fourth landmark, the dome of the liver, the difference was statistically significant for two of three of the test groups.

Table 2 presents interexpert variability data and the results of sign test in the same format as that of Table 1. Unlike in the case of the direct method, the sign test showed statistically significant differences between the reference group and the test groups, when landmarks were pooled together. Treated separately, statistically significant differences were found between the reference group and one or more test groups for each of the four landmarks. Data presented in these two tables clearly show that the direct method was superior to indirect method. Moreover, except for the identification of the dome of the liver, the direct method performed as well as the experts.

The average execution times for direct registration and indirect registration were 130 ± 36 and 124 ± 34 s, respectively. This was approximately 30 times faster than times required for a pure software implementation on the same host PC.

DISCUSSION

If aligned correctly, the fusion of archived preprocedural PET and the intraprocedural volumetric CT can achieve almost every aspect of an ideal intraprocedural imaging modality for cancer treatment interventions: highlighted tumor with clear delineation of surrounding anatomy, multiplanar and interactive visualization capabilities³⁶, low radiation exposure risk, and no special ablation instrument during the procedure.³⁷ Unfortunately, the functional information from PET, even when available on the picture archiving and communication system, remains unavailable on image-guidance workstations in interventional pro-

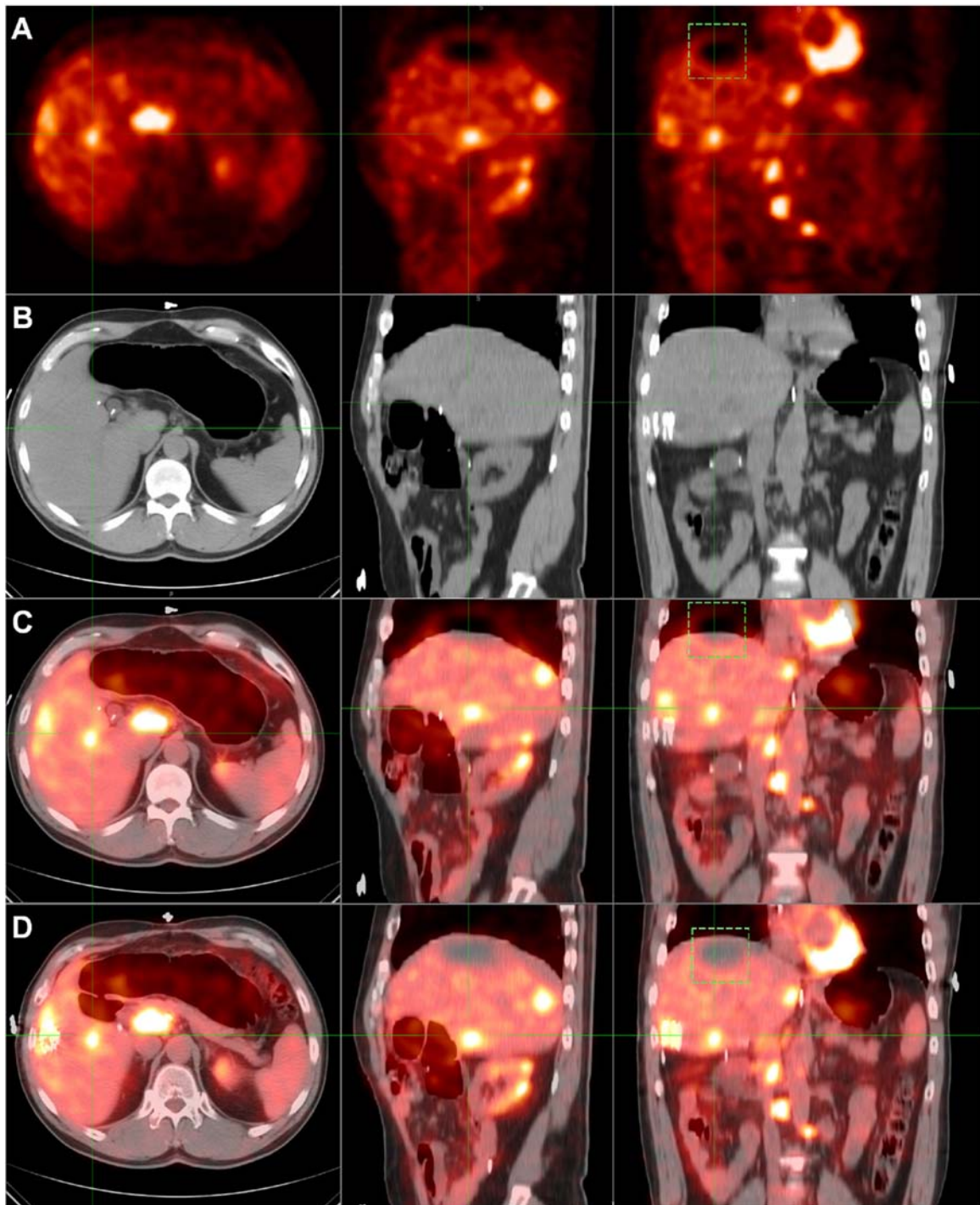


Fig 5. Registration of PET and CT images acquired from separate scanners in a 56-year-old patient with a colorectal tumor and three hepatic metastases. a PET image. b Corresponding CT image before registration. c PET-CT fusion image before registration. d PET-CT fusion image after nonrigid registration. *Green rectangle* indicates the spatial alignment of edges.

Table 1. Direct Method: Interexpert Variability in Landmark Identification Across 18 Image Pairs

Landmark	Median interexpert variability in landmark identification (mm) (IQR) [<i>P</i> value ^a]			
	Reference group ^b	Group 1 ^c	Group 2 ^d	Group 3 ^e
Dome of liver	6.6 (6.3–7.0)	6.8 (6.3–7.6) [<i>P</i> = 0.24]	7.3 (6.7–7.8) [<i>P</i> < 0.01]	7.1 (6.8–7.5) [<i>P</i> < 0.01]
Inferior tip of liver	6.7 (5.6–7.4)	6.9 (6.6–7.2) [<i>P</i> = 0.05]	6.9 (6.6–7.4) [<i>P</i> = 0.12]	7.2 (6.2–7.5) [<i>P</i> = 0.24]
Upper pole of kidney	6.2 (6.0–7.0)	6.4 (5.8–6.9) [<i>P</i> = 0.24]	6.1 (5.8–6.5) [<i>P</i> = 0.95]	6.2 (5.8–6.9) [<i>P</i> = 0.59]
Lower pole of kidney	5.5 (5.1–6.1)	5.7 (5.0–5.8) [<i>P</i> = 0.41]	5.6 (5.1–5.8) [<i>P</i> = 0.59]	5.8 (5.5–6.1) [<i>P</i> = 0.02]
Overall	6.2 (5.6–6.9)	6.5 (5.8–7.0) [<i>P</i> = 0.02]	6.4 (5.7–7.2) [<i>P</i> = 0.14]	6.6 (5.8–7.2) [<i>P</i> = 0.10]

IQR interquartile range

^a*P* value is from one-sided sign test evaluating if the median distance between locations in the group is less than or equal to the median distance between locations in the reference group

^bReference group: PET₁, PET₂, PET₃

^cGroup 1: PET_{ALGO}, PET₂, PET₃

^dGroup 2: PET₁, PET_{ALGO}, PET₃

^eGroup 3: PET₁, PET₂, PET_{ALGO}

cedure suites, mainly because it is not spatially coupled with the ongoing guidance roadmap, the CT. We have proposed a workflow for combining PET and CT, with hardware acceleration that removes current barriers to dual-modality roadmapping. The off-line implementation of the workflow in this work that required minimal alterations to the current practice and made use of the preprocedural PET or PET/CT and intraprocedural NCCT routinely acquired for RFA of hepatic metastases proves its clinical viability. The workflow could therefore be implemented clinically.

Is Hybrid PET/CT Scanner a Solution?

The benefits of PET guidance in breast biopsy are well documented^{38,39} and are being recognized for hepatic RFA.¹⁴ Only a few preliminary attempts,

however, have been made to exploit these benefits so far.^{37,40}

One of the first attempts to incorporate PET into hepatic RFA made use of a hybrid PET/CT scanner, which achieves image registration by sequential PET and CT scanning during a single session. In this recent case study, Prior et al. performed RFA of a CT-invisible metastatic hepatic lesion of a patient.⁴⁰ Although not used to guide the RF applicator interactively into the targeted tumor, PET scanning was performed once to confirm appropriate placement of a customized PET-visible applicator introducer. Negative 1-day and 3-month follow-up PET/CT scans confirmed successful ablation. This case study did not address the inherent limitations of hybrid PET/CT scanning (slow speed, radiation exposure, misregistration from breathing⁴¹, and inability to repeat PET

Table 2. Indirect Method: Interexpert Variability in Landmark Identification Across 18 Image Pairs

Landmark	Median interexpert variability in landmark identification (mm) (IQR) [<i>P</i> value ^a]			
	Reference group ^b	Group 1 ^c	Group 2 ^d	Group 3 ^e
Dome of liver	6.6 (6.3–7.0)	7.9 (7.6–8.3) [<i>P</i> < 0.01]	8.2 (7.5–8.5) [<i>P</i> < 0.01]	8.1 (7.5–8.7) [<i>P</i> < 0.01]
Inferior tip of liver	6.7 (5.6–7.4)	7.0 (6.7–8.0) [<i>P</i> = 0.12]	7.1 (6.7–7.8) [<i>P</i> = 0.05]	7.5 (7.0–8.4) [<i>P</i> < 0.01]
Upper pole of kidney	6.2 (6.0–7.0)	7.1 (6.5–7.5) [<i>P</i> < 0.01]	6.8 (6.3–7.2) [<i>P</i> = 0.02]	7.1 (6.7–7.6) [<i>P</i> < 0.01]
Lower pole of kidney	5.5 (5.1–6.1)	5.7 (5.3–6.3) [<i>P</i> = 0.12]	5.8 (5.4–6.4) [<i>P</i> = 0.05]	6.2 (5.7–6.4) [<i>P</i> < 0.01]
Overall	6.2 (5.6–6.9)	7.0 (6.3–7.9) [<i>P</i> < 0.01]	6.9 (6.3–7.8) [<i>P</i> < 0.01]	7.2 (6.4–8.0) [<i>P</i> < 0.01]

IQR interquartile range

^a*P* value is from one-sided sign test evaluating if the median distance between locations in the group is less than or equal to the median distance between locations in the reference group

^bReference group: PET₁, PET₂, PET₃

^cGroup 1: PET_{ALGO}, PET₂, PET₃

^dGroup 2: PET₁, PET_{ALGO}, PET₃

^eGroup 3: PET₁, PET₂, PET_{ALGO}

scanning). The use of the hybrid PET/CT scanner also prolonged the procedure considerably. Although this study underscored the merits of incorporating PET into RFA procedures, the methodology remains impractical for routine clinical use because, as Wong et al.⁴² have noted, the hybrid PET/CT scanner's purpose and design are diagnostic-centric, not interventional-centric.

Performance of Algorithmic PET/CT Registration in RFA

Because real-time PET imaging during RFA is not practical and is technologically challenging, a second alternative is to incorporate existing (preprocedural) PET images through retrospective registration. Our study took the algorithmic approach^{23,26} together with hardware acceleration²⁸ to evaluate the feasibility of registering preprocedural PET and intraprocedural NCCT images. Compared with prior PET–CT registration studies, a similar registration of PET and CT images from RFA procedures is more challenging because of the relatively poor quality of intraprocedural NCCT images. In a patient cohort with hepatic metastases, our two registration methods (direct and indirect) provided acceptable accuracy, given PET's 5–7-mm spatial resolution and the current practice of adding a 10-mm treatment margin to hepatic metastases.^{43–45}

This investigation constitutes the critical proof of concept for the future goal of incorporating preprocedural PET into NCCT guidance of hepatic RFA. It was for this reason that all images were obtained from actual hepatic RFA procedures. However, the retrospective nature of our study also presented a few limitations. First, the intraprocedural NCCT scans did not perfectly simulate the NCCT scans that the proposed system would gather. Out of multiple NCCT scans during an RFA procedure, only the very first scan, acquired before insertion of the RF applicator, had sufficient volumetric coverage for PET–CT registration. Consistent with current practice, most other intraprocedural CT scans contained no more than four axial slices, which were too few to perform algorithmic registration.

The intraprocedural NCCT images included in this study did not show the RF applicator and any applicator-induced metal artifacts but were otherwise similar to images acquired with the applica-

tor. To evaluate the effect of metal artifacts, an additional case was identified in which a full liver NCCT scan contained metal artifacts. Registration in this case was performed twice, by first keeping and then excluding regions of metal artifacts from the registration process. The final results for these two situations showed only submillimeter difference in registration accuracy.

Quantitative evaluation of multimodality image registration of clinical images is always a challenge. The problem is compounded for lower-resolution images, such as those acquired with PET that lack clearly identifiable anatomic landmarks. Most PET–CT registration studies have therefore used expert opinions, such as semiquantitative visual scoring assessment of alignment of anatomic edges^{21,22} and expert-defined registration.²³ A similar validation approach was used in this study, which evaluated the overall alignment of liver and kidney. We further assumed that the alignment of organ edges meant the alignment of structures in the liver parenchyma. Judging visually, no misalignment of structures within the hepatic parenchyma was observed in any of the 18 cases. Because metastatic tumors are often invisible in NCCT (among the basic motivations for this study), those could not be used for validation. However, two repeat cases showed unambiguously identifiable anatomic landmarks (prior ablation zones) in both PET and NCCT. The accurate spatial alignment of these landmarks, as shown in Figure 6, reinforces the validity of our assumption and also demonstrates accurate registration inside the liver.

Direct or Indirect?

Two registration strategies were investigated in this study. The direct method was more accurate, because it was not affected by any breathing-induced misregistration between PET and CT components of the hybrid PET/CT scan and directly reflects the current anatomy. If direct registration is possible, this is the optimal strategy. However, the direct method may not be as robust as the indirect method because of the low resolution and low SNR of PET images. In fact, before hybrid PET/CT scanners became prevalent, registration of PET and CT images from stand-alone scanners was accomplished mostly by registering the CT with the transmission PET scan,

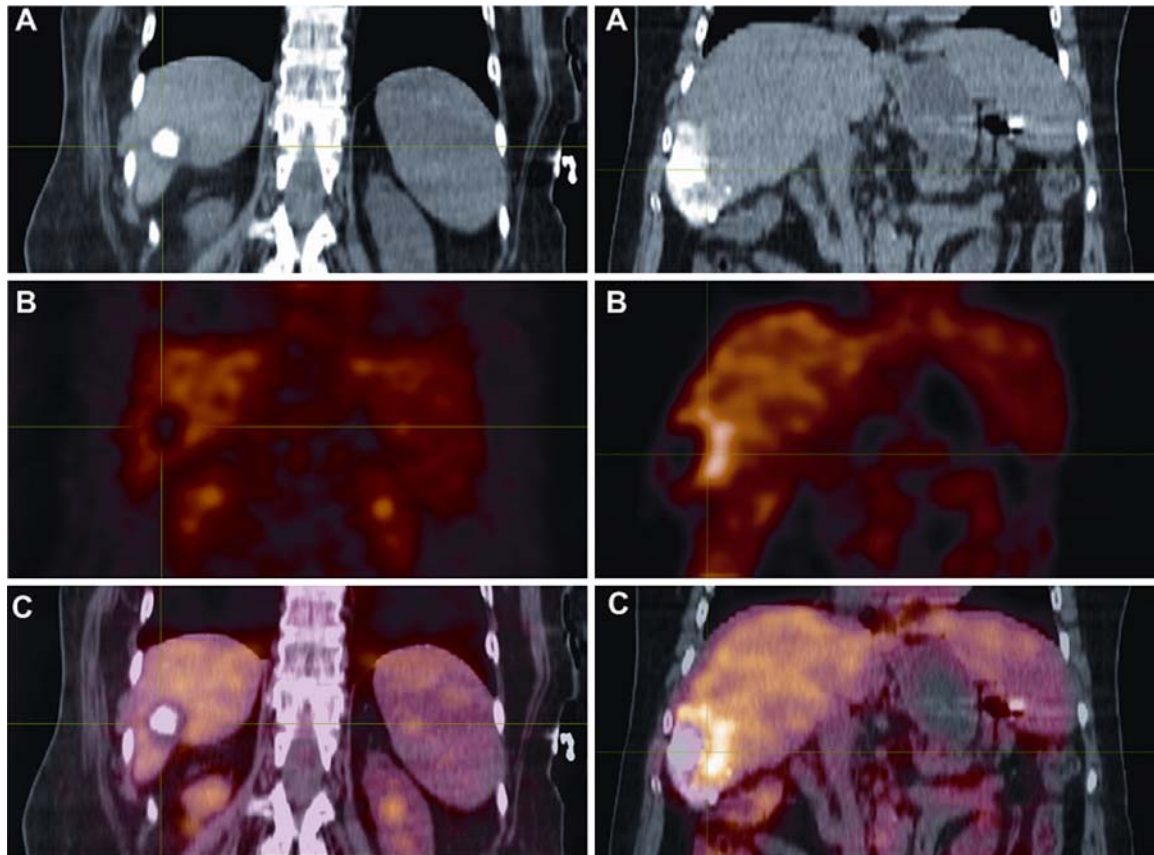


Fig 6. Two examples illustrating the accuracy of nonrigid registration at an intrahepatic location. The case in the *left column* shows the center alignment of treatment scar. The case in the *right column* shows the edge alignment of treatment scar and residual tumor. a CT image. b Registered PET image. c PET–CT fusion after registration. The intersection of crosshairs indicates common structures.

the counterpart of the preprocedural CT (from hybrid PET/CT scanner) in this study. Thus, the essence of the PET–CT registration algorithms was actually an intramodality registration. Mattes et al. used the CT scan to register with the PET transmission scan from different scanners and successfully achieved PET–CT registration in the chest.²² However, large registration errors were observed in the abdomen, which indicates that the anatomy moved significantly between transmission and emission PET. The indirect method could be a potential alternative (or an intermediate step) for the direct method in extremely adverse conditions that have very large deformation, small image volume, or very low image quality. In such cases, PET and CT components of a hybrid PET/CT scan can be preregistered to compensate for breathing-induced misalignments, although multiple registrations could lead to considerable interpolation artifacts.

Future Work

Our results indicate that accurate registration between preprocedural PET and intraprocedural NCCT can be achieved in a rapid manner. Moreover, the fully automatic nature of our registration is critical for eventual clinical implementation. Although our hardware-accelerated implementation of nonrigid image registration is drastically faster than software-only implementations, further acceleration will be needed. Because our algorithm decomposes the problem to registration of several subvolumes, a potential strategy can be to employ multiple FPGAs to register subvolume in parallel, because their registrations are independent of each other. It is reasonable to expect that the speedup of the multi-FPGA implementation would achieve nearly linear speedup. Our future efforts will also include testing the registration algorithm with low-

dose intraprocedural NCCT scans as well as studying more thoroughly image registration in the presence of RF applicator-caused metal artifacts.

CONCLUSIONS

In summary, the methodology we have presented for PET augmentation of CT for guiding RFA of hepatic metastases is accurate, fast, performance scalable, and clinically viable. PET-augmented CT images have the potential to allow precise placement of the RF applicator in the tumor. The information-rich fusion image may also shorten the procedure time by optimizing initial RF probe placement. Upon clinical translation, the improved tumor targeting technology we describe here could enable complete and definitive ablation of hepatic metastases, potentially reducing high recurrence rates and the large number of repeat ablations currently observed while simultaneously improving long-term survival. Improved intraprocedural visualization is also expected to expand the application of RFA to patients with tumors difficult to reach with current technology.

REFERENCES

1. Bilchik AJ, Wood TF, Allegra DP: Radiofrequency ablation of unresectable hepatic malignancies: lessons learned. *Oncologist* 6:24–33, 2001
2. Veit P, Antoch G, Stergar H, Bockisch A, Forsting M, Kuehl H: Detection of residual tumor after radiofrequency ablation of liver metastasis with dual-modality PET/CT: initial results. *Eur Radiol* 16:80–87, 2006
3. Dupuy DE, Goldberg SN: Image-guided radiofrequency tumor ablation: challenges and opportunities—part II. *J Vasc Interv Radiol* 12:1135–1148, 2001
4. McGhana JP, Dodd 3rd, GD: Radiofrequency ablation of the liver: current status. *AJR Am J Roentgenol* 176:3–16, 2001
5. Solbiati L, et al: Percutaneous radio-frequency ablation of hepatic metastases from colorectal cancer: long-term results in 117 patients. *Radiology* 221:159–166, 2001
6. Ng KK, Lam CM, Poon RT, Ai V, Tso WK, Fan ST: Thermal ablation therapy for malignant liver tumors: a critical appraisal. *J Gastroenterol Hepatol* 18:616–629, 2003
7. Antoch G, Kuehl H, Vogt FM, Debatin JF, Stattaus J: Value of CT volume imaging for optimal placement of radiofrequency ablation probes in liver lesions. *J Vasc Interv Radiol* 13:1155–1161, 2002
8. Roman CD, Martin WH, Delbeke D: Incremental value of fusion imaging with integrated PET–CT in oncology. *Clin Nucl Med* 30:470–477, 2005
9. Higgins H, Berger DL: RFA for liver tumors: does it really work? *Oncologist* 11:801–808, 2006
10. Choi J: Imaging of hepatic metastases. *Cancer Control* 13:6–12, 2006
11. Chua SC, et al: The impact of ^{18}F -FDG PET/CT in patients with liver metastases. *Eur J Nucl Med Mol Imaging* 34:1906–1914, 2007
12. Kinkel K, Lu Y, Both M, Warren RS, Thoeni RF: Detection of hepatic metastases from cancers of the gastrointestinal tract by using noninvasive imaging methods (US, CT, MR imaging, PET): a meta-analysis. *Radiology* 224:748–756, 2002
13. Vassiliades VG, et al: Hepatic metastases: CT versus MR imaging at 1.5 T. *Gastrointest Radiol* 16:159–163, 1991
14. Veit P, Kuehle C, Beyer T, Kuehl H, Bockisch A, Antoch G: Accuracy of combined PET/CT in image-guided interventions of liver lesions: an ex-vivo study. *World J Gastroenterol* 12:2388–2393, 2006
15. Townsend DW, Carney JP, Yap JT, Hall NC: PET/CT today and tomorrow. *J Nucl Med* 45(Suppl 1):4S–14S, 2004
16. Solomon SB: Incorporating CT, MR imaging, and positron emission tomography into minimally invasive therapies. *J Vasc Interv Radiol* 16:445–447, 2005
17. Wahl RL, Quint LE, Cieslak RD, Aisen AM, Koeppe RA, Meyer CR: “Anatometabolic” tumor imaging: fusion of FDG PET with CT or MRI to localize foci of increased activity. *J Nucl Med* 34:1190–1197, 1993
18. Hawkes DJ, et al: Tissue deformation and shape models in image-guided interventions: a discussion paper. *Med Image Anal* 9:163–175, 2005
19. Maes F, Collignon A, Vandermeulen D, Marchal G, Suetens P: Multimodality image registration by maximization of mutual information. *IEEE Trans Med Imaging* 16:187–198, 1997
20. Pluim JP, Maintz JB, Viergever MA: Mutual-information-based registration of medical images: a survey. *IEEE Trans Med Imaging* 22:986–1004, 2003
21. Camara O, Delso G, Colliot O, Moreno-Ingelmo A, Bloch I: Explicit incorporation of prior anatomical information into a nonrigid registration of thoracic and abdominal CT and ^{18}F -FDG whole-body emission PET images. *IEEE Trans Med Imaging* 26:164–178, 2007
22. Mattes D, Haynor DR, Vesselle H, Lewellen TK, Eubank W: PET–CT image registration in the chest using free-form deformations. *IEEE Trans Med Imaging* 22:120–128, 2003
23. Shekhar R, et al: Automated 3-dimensional elastic registration of whole-body PET and CT from separate or combined scanners. *J Nucl Med* 46:1488–1496, 2005
24. Meyer CR, et al: Demonstration of accuracy and clinical versatility of mutual information for automatic multimodality image fusion using affine and thin-plate spline warped geometric deformations. *Med Image Anal* 1:195–206, 1997
25. Slomka PJ, Dey D, Przetak C, Aladl UE, Baum RP: Automated 3-dimensional registration of stand-alone (^{18}F -FDG whole-body PET with CT. *J Nucl Med* 44:1156–1167, 2003
26. Walimbe V, Shekhar R: Automatic elastic image registration by interpolation of 3D rotations and translations from discrete rigid-body transformations. *Med Image Anal* 10:899–914, 2006
27. Dandekar O, Shekhar R: Image registration accuracy with low-dose CT: How low can we go? *Proc. IEEE*

International Symposium on Biomedical Imaging, Arlington, VA, USA, April 6–9, 2006

28. Dandekar O, Shekhar R: FPGA-accelerated deformable image registration for improved target-delineation during CT-guided interventions. *IEEE Trans Biomed Circuits Syst* 1:116–127, 2007

29. Studholme C, Hill DLG, Hawkes DJ: An overlap invariant entropy measure of 3D medical image alignment. *Pattern Recogn* 32:71–86, 1999

30. Shoemake K: Quaternion calculus and fast animation. *SIGGRAPH Course Notes* 10:101–121, 1987

31. Dandekar O, Castro-Pareja C, Shekhar R: FPGA-based real-time 3D image preprocessing for image-guided medical interventions. *J Real-Time Image Process* 1:285–301, 2007

32. Perona P, Malik J: Scale-space and edge-detection using anisotropic diffusion. *IEEE Trans Pattern Anal Mach Intell* 12:629–639, 1990

33. Goerres GW, Burger C, Schwitter MR, Heidelberg TN, Seifert B, von Schulthess GK: PET/CT of the abdomen: optimizing the patient breathing pattern. *Eur Radiol* 13:734–739, 2003

34. Castro-Pareja CR, Jagadeesh JM, Shekhar R: FAIR: a hardware architecture for real-time 3-D image registration. *IEEE Trans Inf Technol Biomed* 7:426–434, 2003

35. Dandekar O, Plishker W, Bhattacharyya SS, Shekhar R: Multiobjective optimization for reconfigurable implementation of medical image registration. *Int J Reconfigurable Comput*, 2008. doi:10.1155/2008/738174

36. Goldberg SN, et al: Image-guided tumor ablation: standardization of terminology and reporting criteria. *Radiology* 235:728–739, 2005

37. Wood BJ, et al: Technologies for guidance of radio-frequency ablation in the multimodality interventional suite of the future. *J Vasc Interv Radiol* 18:9–24, 2007

38. Khalkhali I, Mishkin FS, Diggles LE, Klein SR: Radionuclide-guided stereotactic prebiopsy localization of non-palpable breast lesions with normal mammograms. *J Nucl Med* 38:1019–1022, 1997

39. Raylman RR, et al: Positron emission mammography-guided breast biopsy. *J Nucl Med* 42:960–966, 2001

40. Prior JO, Kosinski M, Delaloye AB, Denys A: Initial report of PET/CT-guided radiofrequency ablation of liver metastases. *J Vasc Interv Radiol* 18:801–803, 2007

41. Goerres GW, Kamel E, Heidelberg TN, Schwitter MR, Burger C, von Schulthess GK: PET-CT image co-registration in the thorax: influence of respiration. *Eur J Nucl Med Mol Imaging* 29:351–360, 2002

42. Wong K, et al: PET/CT-guided interventional procedures: rationale, justification, initial study, and research plan. *Int J CARS* 2:S146–S151, 2007

43. Lodge MA, et al: Developments in nuclear cardiology: transition from single photon emission computed tomography to positron emission tomography-computed tomography. *J Invasive Cardiol* 17:491–496, 2005

44. Elias D, et al: Resection of liver metastases from colorectal cancer: the real impact of the surgical margin. *Eur J Surg Oncol* 24:174–179, 1998

45. Shirabe K, et al: Analysis of prognostic risk factors in hepatic resection for metastatic colorectal carcinoma with special reference to the surgical margin. *Br J Surg* 84:1077–1080, 1997